

# One-pot synthesis of monodisperse iron oxide nanoparticles for potential biomedical applications\*

Jin Xie<sup>1</sup>, Sheng Peng<sup>1</sup>, Nathan Brower<sup>1</sup>, Nader Pourmand<sup>2</sup>,  
Shan X. Wang<sup>3</sup>, and Shouheng Sun<sup>1,‡</sup>

<sup>1</sup>Department of Chemistry, Brown University, Providence, RI 02912, USA;

<sup>2</sup>Stanford Genome Technology Center, 855 California Ave., Palo Alto, CA 94304, USA;

<sup>3</sup>Department of Materials Science and Engineering and Department of Electrical Engineering, Stanford University, Stanford, CA 94305, USA

**Abstract:** One-pot reaction of iron(III) acetylacetonate, Fe(acac)<sub>3</sub>, [or Fe(acac)<sub>3</sub> and M(acac)<sub>2</sub> where M = Mn and Co], with 1,2-alkanediol, oleic acid, and oleylamine in high boiling organic solvent leads to monodisperse ferrite MFe<sub>2</sub>O<sub>4</sub> nanoparticles. Depending on the concentration of the metal precursors, surfactant-to-metal precursor ratio and the solvent used in the reaction, the particle size from this one-pot reaction can be tuned from 4 to 15 nm. The as-synthesized iron oxide nanoparticles have an inverse spinel structure, and their magnetic properties are controlled by particle size and M in the MFe<sub>2</sub>O<sub>4</sub> structure. The hydrophobic iron oxide nanoparticles are readily transformed into hydrophilic ones by functional phospholipid addition to the as-synthesized particles and as a result, the monodisperse nanoparticles are readily functionalized with biotin, –COOH, –SH, and –NH<sub>2</sub>, facilitating their link to biomolecules for biomedical applications.

**Keywords:** ferrite nanoparticles; chemical synthesis; surface functionalization; phospholipid coating; biomedical applications.

## INTRODUCTION

Magnetic nanoparticles with size up to 20 nm in diameter represent an important class of artificial nanostructured materials. Their magnetic properties change drastically with the sizes as magnetic anisotropic energy,  $KV$ , where  $K$  is the magnetic anisotropic constant and  $V$  is the particle volume, becomes comparable to the thermal energy,  $kT$ , resulting in moment randomization and superparamagnetism [1,2]. Such superparamagnetic nanoparticles have great potential for biomedical applications [3–8]. Their magnetic signal far exceeds that from any of the known bio-entities, making them readily identified in the ocean of biomolecules. Without external magnetic field, they show no net magnetic moment, facilitating their long-term stability in various dispersion media. They are smaller than or comparable to a cell (10–100 nm), a virus (20–450 nm), a protein (5–50 nm), or a gene (2 nm wide and 10–100 nm long). These, plus their capability of being manipulated under an external magnetic field, provide controllable means of magnetically tagging of all biomolecules, leading to highly efficient

\*Paper presented at the 40<sup>th</sup> IUPAC Congress, Beijing, China, 14–19 August 2005. Other presentations are published in this issue, pp. 889–1090.

‡Corresponding author: E-mail: ssun@brown.edu

bioseparation/biodelivery [7] and highly sensitive biolabeling and magnetic resonance imaging (MRI) contrast enhancement [8–10].

To apply superparamagnetic nanoparticles for biomedical applications, the nanoparticles should be monodisperse to have uniform physical and chemical properties for controlled biodistribution, bio-elimination, and contrast effects. The magnetic nanoparticles should also have high magnetic moment, and can be so modified that they are capable of binding specifically to a biological entity and able to withstand various physiological conditions. Iron oxide nanoparticles, due to their chemical and magnetic stability and low level of toxicity in biological systems, have been widely tested for their use in biomedicine [3]. However, some well-known material problems need to be solved before these nanoparticles can be utilized for any practical applications. The iron oxide nanoparticles used for the tests are often polydisperse with large variation not only in size, but also in shape. Consequently, the physical and chemical properties of these particles are not well controlled, and important data on biodistribution/bioelimination in biological systems, which are essential for *in vivo* applications, are currently difficult to obtain.

Monodisperse ferrite  $\text{MFe}_2\text{O}_4$  nanoparticles were recently made by a high-temperature reduction/decomposition reaction of metal acetylacetonate [11–13]. The size of the particles was controlled up to 8 nm from the one-step reduction/decomposition reaction. Larger size, up to 20 nm, was made possible by seed-mediated growth in which small  $\text{MFe}_2\text{O}_4$  nanoparticles were used as seeds and more  $\text{MFe}_2\text{O}_4$  was coated over the seeds. By controlling the heating parameters, the reaction further led to the ferrite nanoparticles with cube- or polyhedron-like shapes [13,14]. This reduction/decomposition synthesis is complimentary to other reports in iron oxide nanoparticle syntheses from high-temperature decomposition reactions [15–21]. The iron precursors used in this new synthesis are commercially readily available and less toxic than the iron pentacarbonyl,  $\text{Fe}(\text{CO})_5$ , a common precursor used in thermal decomposition reaction. However, the synthesis of larger nanoparticles (>10 nm) via seed-mediated growth method involves multiple-step syntheses and as a result, the process leading to 15–20 nm nanoparticles is time-consuming. It is desired that, for practical applications, the iron oxide nanoparticles with a range of sizes can be prepared via a one-step synthesis. Here we report a one-pot reaction of metal acetylacetonate with polyol in the presence of oleic and oleylamine to prepare  $\text{Fe}_3\text{O}_4$ ,  $\text{MnFe}_2\text{O}_4$ , and  $\text{CoFe}_2\text{O}_4$  nanoparticles with the size tunable from 5 to 15 nm. We further demonstrate that these nanoparticles are magnetically stable and can be readily functionalized for potential biomedical applications.

## EXPERIMENTAL SECTION

The synthesis was carried out using standard airless procedures and commercially available reagents. Absolute ethanol and hexane were used as received. Phenyl ether (99 %), benzyl ether (99 %), 1-octadecene (90 %), 1,2-hexadecanediol (90 %), 1,2-tetradecanediol (97 %), oleic acid (90 %), oleylamine (>70 %), D-(+)-glucose, and HABA/avidin reagent were purchased from Aldrich Chemical Company. Iron(III) acetylacetonate [ $\text{Fe}(\text{acac})_3$ ], cobalt(II) acetylacetonate [ $\text{Co}(\text{acac})_2$ ], and manganese(II) acetylacetonate [ $\text{Mn}(\text{acac})_2$ ] were from Strem Chemicals, Inc. 1,2-Distearoyl-sn-glycero-3-phosphoethanolamine-*N*-[biotinyl(polyethylene glycol)2000], DSPE-PEG(2000)Biotin, was obtained from Avanti Polar Lipids. Nanosep 100 k Omega centrifugal device was from Fisher Scientific.

### One-pot reaction to 6 nm $\text{Fe}_3\text{O}_4$ nanoparticles

$\text{Fe}(\text{acac})_3$  (2 mmol), 1,2-hexadecanediol (10 mmol), oleic acid (6 mmol), and oleyl amine (6 mmol) and benzyl ether (20 mL) were mixed and magnetically stirred under a flow of nitrogen. The mixture was heated to 200 °C for 2 h, and then under a blanket of nitrogen, heated to reflux (300 °C) for 1 h. The black-brown colored mixture was cooled down to room temperature by removing the heat source. Under ambient conditions, ethanol (40 ml) was added to the mixture and a black material was precipi-

tated and separated via centrifugation. The black product was dissolved in hexane in the presence of oleic acid (~0.05 mL) and oleyl amine (~0.05 mL). Centrifugation (6000 rpm, 10 min) was applied to remove any undispersed residue (almost none). The product, 6 nm Fe<sub>3</sub>O<sub>4</sub> nanoparticles, was then precipitated with ethanol, centrifuged (6000 rpm, 10 min) to remove the solvent and redispersed into hexane.

### One-pot reaction to 5 nm CoFe<sub>2</sub>O<sub>4</sub> nanoparticles

Co(acac)<sub>2</sub> (1 mmol), Fe(acac)<sub>3</sub> (2 mmol), 1,2-hexadecanediol (10 mmol), oleic acid (6 mmol), and oleyl amine (6 mmol) and benzyl ether (20 mL) were mixed and magnetically stirred under a flow of nitrogen. The mixture was heated to 200 °C for 2 h, and then, under a blanket of nitrogen, heated to reflux (~300 °C) for 1 h. The black colored mixture was cooled down to room temperature by removing the heat source. Following the work-up procedures described in the synthesis of 6 nm Fe<sub>3</sub>O<sub>4</sub> nanoparticles, a black–brown hexane dispersion of 5 nm CoFe<sub>2</sub>O<sub>4</sub> nanoparticles was produced.

### One-pot reaction to 7 nm MnFe<sub>2</sub>O<sub>4</sub> nanoparticles

Mn(acac)<sub>2</sub> (1 mmol) Fe(acac)<sub>3</sub> (2 mmol), 1,2-hexadecanediol (10 mmol), oleic acid (6 mmol), and oleyl amine (6 mmol) and benzyl ether (20 mL) were mixed and magnetically stirred under a flow of nitrogen. The mixture was heated to 200 °C for 2 h, and then, under a blanket of nitrogen, heated to reflux (~300 °C) for 1 h. The black colored mixture was cooled down to room temperature by removing the heat source. Following the work-up procedures described in the synthesis of 6 nm Fe<sub>3</sub>O<sub>4</sub> nanoparticles, a black–brown hexane dispersion of 7 nm MnFe<sub>2</sub>O<sub>4</sub> nanoparticles was produced.

Iron oxide nanoparticles with different sizes were made from a similar one-pot reaction by choosing different solvent for the reaction, or by controlling the concentration of the metal precursors and metal/surfactant ratio. The particles up to 15 nm in diameter had been produced.

### Surface modification of the iron oxide nanoparticles

The solvent hexane was evaporated from the hexane dispersion of the particles under a flow of nitrogen gas, giving black solid residue of iron oxide nanoparticles. The residue was dissolved in chloroform to form the chloroform dispersion at a concentration of 0.5 mg particles/mL solution. 1 mL of chloroform solution of DSPE-PEG(2000)Biotin (10 mg/mL) was added into a 2 mL of the nanoparticle dispersion. The mixture was shaken for 1 h, the chloroform solvent was evaporated under nitrogen gas. The solid residue was dispersed in phosphate buffered saline (PBS) solution for further test. A small portion of undispersed residue was filtered off by a 0.2- $\mu$ m syringe filter. The free DSPE-PEG(2000)Biotin was removed by a Nanosep 100 k Omega.

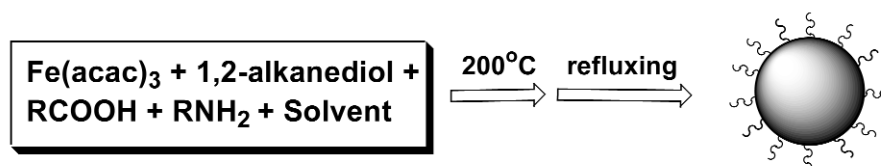
### Nanoparticle characterization

Samples for transmission electron microscopy (TEM) analysis were prepared by drying a hexane dispersion of the particles on amorphous carbon-coated copper grids. The particles were imaged using a Philips TEM 420 (120 kV). Quantitative elemental analyses of the nanoparticles were carried out with electron diffraction spectrum (EDS). X-ray powder diffraction patterns of the particle assemblies were collected on a Bruker AXS D8 Advance diffractometer under Cu K $\alpha$  radiation ( $\lambda = 1.5405 \text{ \AA}$ ). Magnetic properties of the particles were studied using a Lakeshore 7404 high-sensitivity vibrating sample magnetometer (VSM) with fields up to 1 T at room temperature. The diameter of the particles (core diameter plus shell thickness) in dispersion was measured using a Malvern Zeta Sizer Nano S-90 dynamic light-scattering (DLS) instrument. UV–vis analysis was performed on a PerkinElmer Lambda 35 UV–Vis spectrometer.

## RESULTS AND DISCUSSION

### One-pot synthesis of Fe<sub>3</sub>O<sub>4</sub> nanoparticles

As illustrated in Scheme 1, the reaction of Fe(acac)<sub>3</sub> with surfactants at high temperature leads to monodisperse Fe<sub>3</sub>O<sub>4</sub> nanoparticles that can be easily isolated from the reaction by-products and the high boiling point ether solvent. The key to monodispersity of the particles is to heat the mixture to 200 °C first and remain at that temperature for 2 h before the temperature is raised to reflux at 265 °C in phenyl ether, or at ~300 °C in benzyl ether, or 310 °C in 1-octadecene. Directly heating the mixture to reflux from room temperature would result in Fe<sub>3</sub>O<sub>4</sub> nanoparticles with wide size distribution from 4 to 20 nm, indicating that the formation of Fe-based nuclei under these reaction conditions is not a fast process.



**Scheme 1**

One-pot reaction of 2 mmol Fe(acac)<sub>3</sub> with 6 mmol of oleic acid, 6 mmol of oleylamine, and 10 mmol of 1,2-hexadecanediol in 20 mL benzyl ether led to 6 nm Fe<sub>3</sub>O<sub>4</sub> nanoparticles, as described in the experimental section. If phenyl ether (or 1-octadecene) was used as solvent, 4 nm (or ~12 nm) Fe<sub>3</sub>O<sub>4</sub> nanoparticles were separated. As the boiling point of 1-octadecene (310 °C), benzyl ether (298 °C) is higher than that of phenyl ether (259 °C), the larger size of Fe<sub>3</sub>O<sub>4</sub> nanoparticles obtained from benzyl ether (or 1-octadecene) solution indicates that high reaction temperature facilitates the formation of large particles. Figures 1A and 1B show two TEM images of 6 nm and ~15 nm Fe<sub>3</sub>O<sub>4</sub> nanoparticles synthesized from benzyl ether, and Fig. 1C is the TEM image of the ~12 nm Fe<sub>3</sub>O<sub>4</sub> particles from 1-octadecene. It can be seen that the one-pot reaction yields nearly monodisperse Fe<sub>3</sub>O<sub>4</sub> nanoparticles.

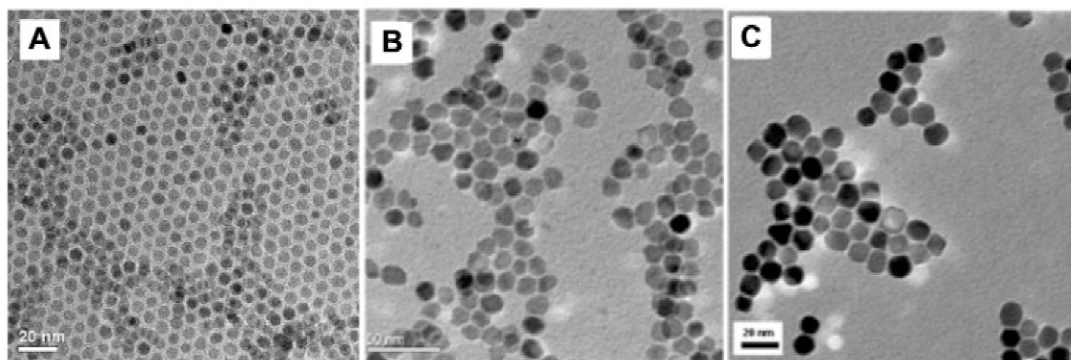


**Fig. 1** TEM images of Fe<sub>3</sub>O<sub>4</sub> nanoparticles prepared from the one-pot reaction: (A) 6 nm Fe<sub>3</sub>O<sub>4</sub> from 20 mL benzyl ether, (B) ~15 nm Fe<sub>3</sub>O<sub>4</sub> from 10 mL benzyl ether, and (C) ~12 nm Fe<sub>3</sub>O<sub>4</sub> nanoparticles from 20 mL 1-octadecene.

If the volume of the benzyl ether solvent used in the one-pot reaction was reduced from 20 to 15 mL, then 8 nm  $\text{Fe}_3\text{O}_4$  nanoparticles were separated. Further reduction in solvent volume to 10 mL led to one-step synthesis of ~15 nm  $\text{Fe}_3\text{O}_4$  nanoparticles, as shown in Fig. 1B.

The amount of surfactant used in the one-pot reaction also affects the size of the  $\text{Fe}_3\text{O}_4$  nanoparticles. In 20 mL benzyl ether solvent, 4 mmol of oleic acid and 4 mmol of oleylamine led to  $\text{Fe}_3\text{O}_4$  nanoparticles with average size at 9 nm, while 12 mmol of oleic acid and 12 mmol of oleylamine resulted in the particles with average size at 4 nm. The size dependence of  $\text{Fe}_3\text{O}_4$  on the volume of benzyl ether and mmols of the surfactant mixture of oleic acid/oleylamine is listed in Table 1. It can be seen that in the one-pot reaction condition described in the experimental section, the size of the  $\text{Fe}_3\text{O}_4$  nanoparticles is independent of the volume of the solvent if the surfactants are 4 mmol each. But in the presence of 6 mmol or more of the surfactant mixture, the size of the particles is clearly affected by the volume of the solvent used in the reaction.

**Table 1** Relationship between the size of  $\text{Fe}_3\text{O}_4$  particles (in nm) and the volume of the solvent (in mL) or the amount of the surfactants (in mmol) used in the one-pot reaction.

	4 mmol	6 mmol	12 mmol
10 ml	NA	15 nm	8 nm
15 ml	Ave. 9 nm	8 nm	7 nm
20 ml	Ave. 9 nm	6 nm	5 nm

The 3:1 surfactant-to-metal ratio seems to be necessary for the one-pot reaction to make monodisperse  $\text{Fe}_3\text{O}_4$  nanoparticles. Reducing the amount of the surfactant leads to particles with wide size distribution and an average size that is almost independent of the volume of the solvent, as shown in the first column of Table 1. This indicates that during the one-pot reaction, 3 equiv or more of the surfactants are needed for the monodispersity control of the final product, suggesting that the formation of the nanoparticles goes through the replacement of the “acac” in  $\text{Fe}(\text{acac})_3$  by 3 equiv of oleic acid/oleylamine.

Different diol has also been tested for the growth of the iron oxide nanoparticles. It was found that the diol with its hydrocarbon chain shorter than 1,2-hexadecanediol tended to yield larger nanoparticles. For examples, in the same one-pot reaction condition described in the synthesis of 6 nm  $\text{Fe}_3\text{O}_4$  nanoparticles, 1,2-tetradecanediol yielded monodisperse 8 nm  $\text{Fe}_3\text{O}_4$  nanoparticles (Fig. 2A) while 1,2-dodecanediol gave 10 nm  $\text{Fe}_3\text{O}_4$  nanoparticles. Further, it was noticed that in a concentrated reaction solution of 10 mL benzyl ether and 1,2-tetradecanediol, the triangle shape of the iron oxide nanoparticles evolved from the reaction, as shown in Fig. 2B. Due to the symmetry control factor, the triangle can only be developed from the growth of (111) plane of the fcc structured iron oxide. It seems that in a concentrated solution containing shorter alkanediol, the growth of the (100) plane is restrained, leading to the particles with triangle shape.

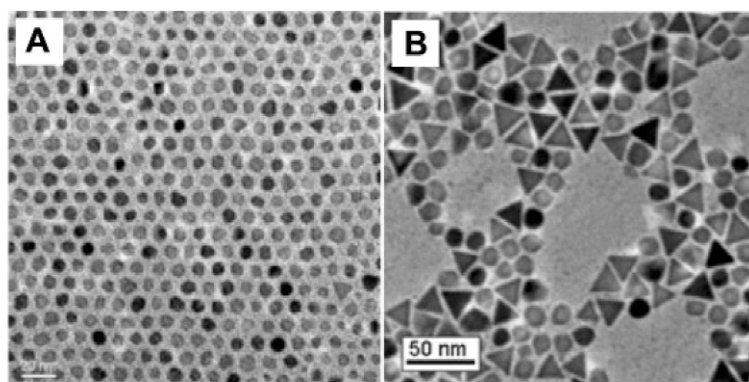
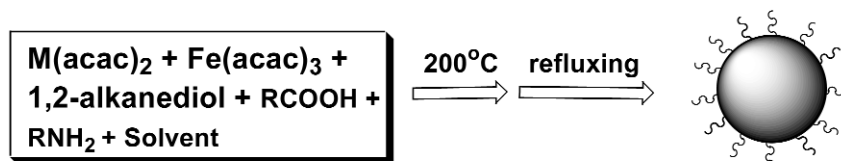


**Fig. 2** TEM images of (A) 8 nm  $\text{Fe}_3\text{O}_4$  nanoparticles using 1,2-tetradecanediol in 20 mL benzyl ether solvent and (B) triangle-shaped  $\text{Fe}_3\text{O}_4$  nanoparticles prepared in 10 mL benzyl ether solvent.

Although the mechanism leading to  $\text{Fe}_3\text{O}_4$  nanoparticles in the one-pot reaction presented here is not completely clear, experimental observations listed above seem to suggest that the formation of iron oxide nanoparticles follows the classical condensation mechanism during the colloidal growth process [22]. An iron oxide particle is built up by the stacking of its respective atomic species. These atomic species are derived from the chemical reaction of partial reduction and decomposition of  $\text{Fe}(\text{oleate})_3$  in the presence of oleylamine. The clustering of the “Fe–O” species gives numerous nuclei that are saturated in the reaction medium (benzyl ether, for example), and aggregate into iron oxide nanoparticles. The solubility of the nuclei in the dispersion decides at what stage the nucleation stops and the aggregation of the nuclei dominates the growth process. The particles cannot be formed if the nuclei are not saturated in the dispersion medium. Above the saturation threshold, the aggregation of the nuclei becomes spontaneous until the particles sinter from the dispersion. In the one-pot reaction synthesis of  $\text{Fe}_3\text{O}_4$  nanoparticles, the reduction in solvent volume leads to the saturation of the oxide-based nuclei at early stage and more reactant can contribute to the growth process, giving larger particles. In larger volume solvent, however, more nuclei are needed to reach saturation at the expense of the iron salt precursor, resulting in smaller  $\text{Fe}_3\text{O}_4$  nanoparticles. The surfactant effect can also be understood in a similar principle. More surfactant is equivalent to a larger volume of solvent and more nuclei are needed to reach the saturation in high surfactant/metal ratio, leading to small nanoparticles.

### One-pot synthesis of $\text{MnFe}_2\text{O}_4$ or $\text{CoFe}_2\text{O}_4$ nanoparticles

The one-pot reaction route to the synthesis of  $\text{Fe}_3\text{O}_4$  nanoparticles illustrated in Scheme 1 can be readily extended to the production of other ferrite nanoparticles with a general formula  $\text{MFe}_2\text{O}_4$ , in which M can be any of Mn, Co, Ni, Mg, Zn, etc. Scheme 2 outlines a general synthetic route to  $\text{MFe}_2\text{O}_4$  nanoparticles.



**Scheme 2**

When  $\text{Co}(\text{acac})_2$  and  $\text{Fe}(\text{acac})_3$  in a 1:2 ratio were mixed in the same one-pot reaction condition as in the synthesis of  $\text{Fe}_3\text{O}_4$ ,  $\text{CoFe}_2\text{O}_4$  nanoparticles were synthesized. Similarly, mixing  $\text{Mn}(\text{acac})_2$  and  $\text{Fe}(\text{acac})_3$  in a 1:2 ratio led to  $\text{MnFe}_2\text{O}_4$  nanoparticles. EDS elemental analysis indicated that the ratio of Co/Fe and Mn/Fe in both cobalt ferrite and manganese ferrite nanoparticles was retained from the ratio of initial metal precursors. The growth of the ferrite nanoparticles seems also to follow the condensation mechanism described in the synthesis of  $\text{Fe}_3\text{O}_4$  nanoparticles as the size of the particles depends on the concentration of the metal salt precursors and the solvent used in the reaction. In the one-pot reaction described in the experimental section, 5 nm  $\text{CoFe}_2\text{O}_4$  nanoparticles were readily separated (Fig. 3A). If the reaction was run in 1-octadecene solvent, then ~11 nm  $\text{CoFe}_2\text{O}_4$  nanoparticles with easily identified shapes were obtained (Fig. 3B). More interestingly, when 1–2 mmol of D-(+)-glucose was present in the 1-octadecene solvent, the quality of the particles was greatly improved and nearly monodisperse  $\text{CoFe}_2\text{O}_4$  nanoparticles were separated, as shown in Fig. 3C. Monodisperse  $\text{MnFe}_2\text{O}_4$  nanoparticles with sizes tunable up to 18 nm can also be prepared similarly.

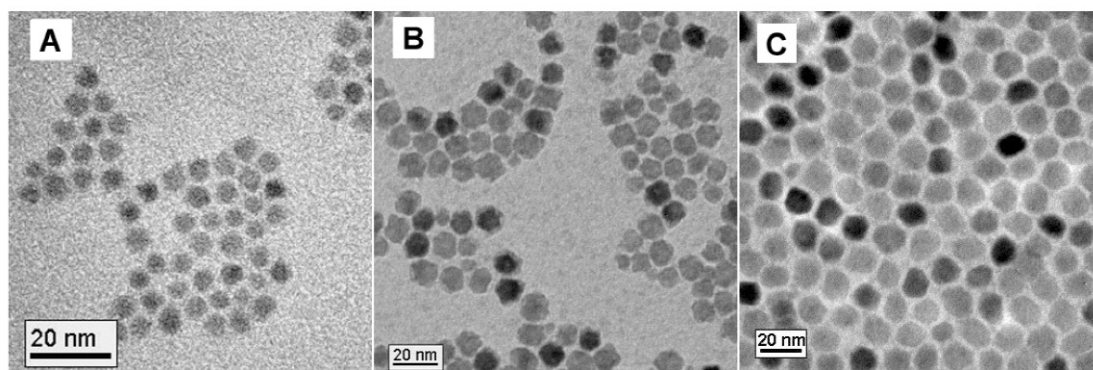


**Fig. 3** TEM images of  $\text{CoFe}_2\text{O}_4$  nanoparticles prepared from the one-pot reaction: (A) 5 nm  $\text{CoFe}_2\text{O}_4$  from 20 mL benzyl ether, (B) ~11 nm  $\text{CoFe}_2\text{O}_4$  from 20 mL 1-octadecene, and (C) ~14 nm  $\text{CoFe}_2\text{O}_4$  from 10 mL 1-octadecene in the presence of 2 mmol of glucose.

### Magnetic properties of the nanoparticles

It is well known that magnetic properties of inverse spinel structured ferrite  $\text{MFe}_2\text{O}_4$  depend on the chemical nature of  $\text{M}^{2+}$ , as  $\text{Fe}^{3+}$  in the structure are evenly distributed in tetrahedral and octahedral interstices within the structure and are antiferromagnetically coupled. Such coupling cancels the moment contribution from  $\text{Fe}^{3+}$ , and the net magnetic moment of the ferrite is solely dependent on  $\text{M}^{2+}$ . Therefore, in  $\text{MFe}_2\text{O}_4$  ferrite series, magnetic moment density of  $\text{Fe}_3\text{O}_4$  or  $\text{MnFe}_2\text{O}_4$  is higher than  $\text{CoFe}_2\text{O}_4$  due to the larger free d-electron contribution from  $\text{Fe}^{2+}$  or  $\text{Mn}^{2+}$ . In the mean time, incorporation of the divalent cation into the Fe–O matrix also changes the magnetic anisotropy of the materials with the incorporation of Co cation in the Fe–O matrix, leading to large magnetic anisotropy and that of Mn cation giving small magnetic anisotropy [23,24].

Figure 4 shows the room-temperature hysteresis loops of ~15 nm  $\text{Fe}_3\text{O}_4$ ,  $\text{MnFe}_2\text{O}_4$ , and  $\text{CoFe}_2\text{O}_4$  nanoparticle assemblies. It shows that both  $\text{Fe}_3\text{O}_4$  and  $\text{MnFe}_2\text{O}_4$  are superparamagnetic at room temperature and their saturation magnetic moments reach over 74 emu/g oxide, while  $\text{CoFe}_2\text{O}_4$  shows ferromagnetic properties with the coercivity at 300 Oe and saturation moment less than 70 emu/g oxide. This is consistent with the inverse spinel structure and magnetic feature of the ferrite materials described above. It was recently demonstrated that superparamagnetic iron oxide nanoparticles at the size of ~10–20 nm could serve as an ideal magnetic label for sensor detection as they possessed high-saturation magnetic moment and zero remanent magnetic moment [25,26]. It can be seen that among three

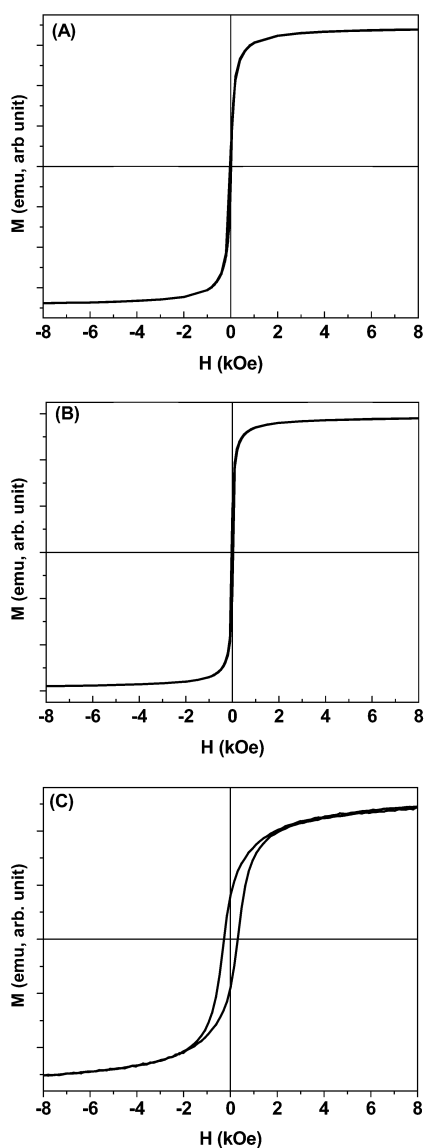


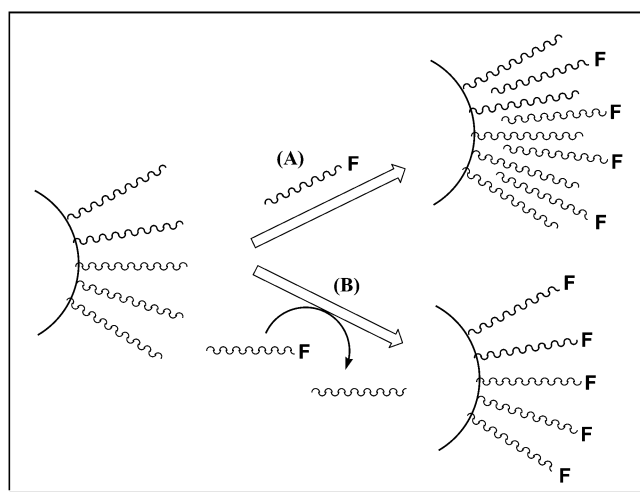
**Fig. 4** Room-temperature hysteresis loop of 15 nm nanoparticles of (A)  $\text{Fe}_3\text{O}_4$ , (B)  $\text{MnFe}_2\text{O}_4$ , and (C)  $\text{CoFe}_2\text{O}_4$ .

ferrite nanoparticle materials reported here,  $\text{Fe}_3\text{O}_4$  and  $\text{MnFe}_2\text{O}_4$  are suitable for magnetic sensor detection.

### Surface modification of iron oxide nanoparticles

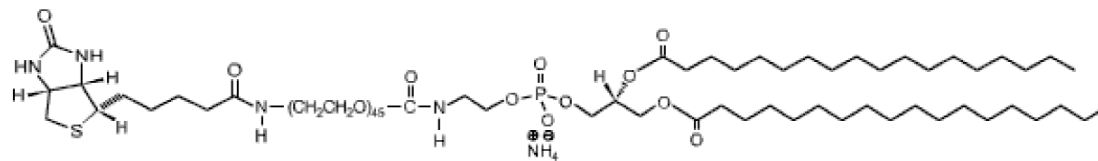
The nanoparticles prepared from Schemes 1 and 2 are coated with a layer of oleate and oleylamine and cannot immediately be used in biological applications because they are only soluble in hexane and other nonpolar or weakly polar organic solvents. For such particles to be useful in biology, they must be soluble in water in a pH range of about 5 to 9, at salt concentrations up to a few hundred mM, and temperatures up to 95 °C for various biological reactions. To meet these biocompatibility requirements, the hydrophobic nanoparticles need to be modified. There are two general approaches in nanoparticle sur-

face functionalization: surfactant addition and surface surfactant exchange [27,28]. The surfactant addition uses the hydrophobic interaction of the incoming long-chain hydrocarbon with that from the surfactant to form a cell-membrane-like double-layer structure, as shown in Scheme 3A. In this approach, the nanoparticles are surrounded by the double-layer structure and the surface of the particles is functionalized with “F”. Depending on the chemical property of “F”, such modified nanoparticles can be dispersed in various liquid media, including water and PBS. Surface surfactant exchange, as shown in Scheme 3B, refers to the replacement of original surfactant on the surface of the particles by a bifunctional surfactant with one functional group capable of binding to the particle surface via strong chemical bond and the other functional group “F” having the polar character so that the particles can be dispersed in water or be further functionalized. Both approaches have been vigorously tested for nanoparticle surface treatment and have shown great potential for biomedical applications [27,28].



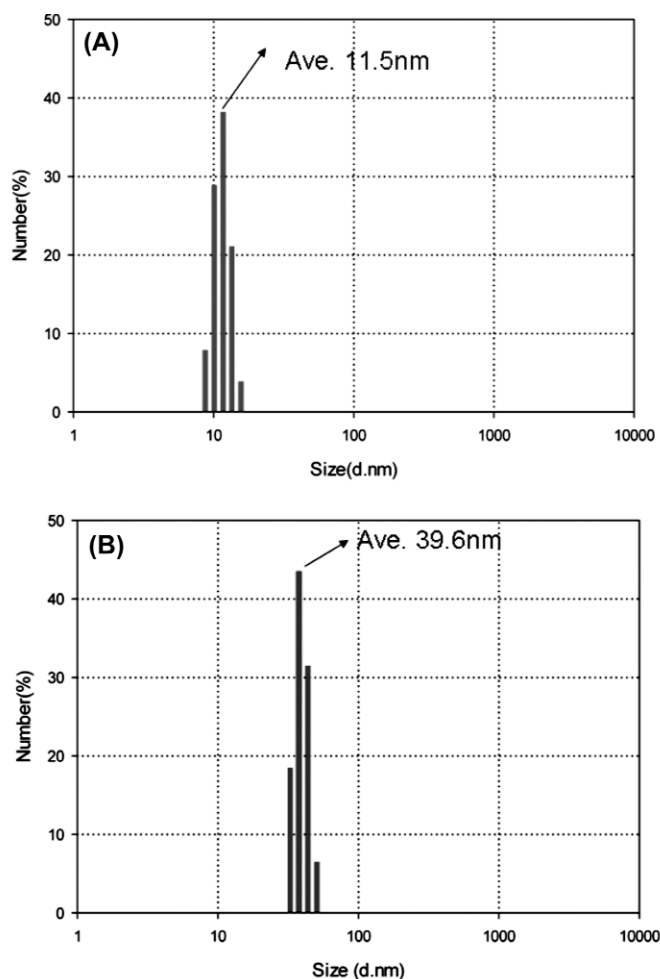
Scheme 3

The addition of a biotinylated-phospholipid, DSPE-PEG(2000)Biotin, shown in Fig. 5, to the hydrocarbon layer of the iron oxide particles gives a robust double-layer structure over the particle surface with the inner layer being original oleate/oleylamine and the outer layer being the phospholipid. DLS measurements (Fig. 6) on the dispersed 8 nm  $\text{Fe}_3\text{O}_4$  nanoparticles show that before surface modification, the nanoparticles have an average hydrodynamic diameter of 11 nm that is close to a simple addition of the particle core diameter (8 nm) and the shell coating (~4 nm). After phospholipid addition, the overall organic shell coating is increased to ~30 nm. This, plus an 8 nm core, gives an overall diameter of 38 nm, while the hydrodynamic diameter of the structure from DLS measurement is at 39.6 nm. Such biotinylated nanoparticles (BNPs) have biotin-functionalized surface and are suitable for streptavidin/avidin attachment.



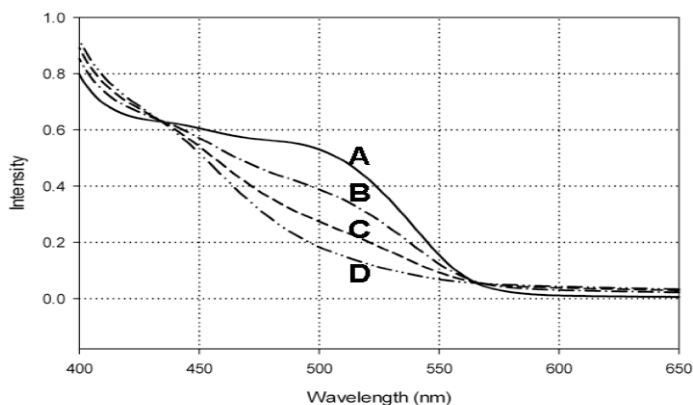
©Avanti Polar Lipids

Fig. 5 Chemical structure of biotinylated phospholipid, DSPE-PEG(2000)Biotin from Avanti Polar Lipids.



**Fig. 6** The hydrodynamic diameter distribution of the Fe<sub>3</sub>O<sub>4</sub> nanoparticles in the dispersion measured by DLS: (A) the as-synthesized 8 nm Fe<sub>3</sub>O<sub>4</sub> nanoparticles in hexane and (B) the particles in water after surface modification with biotinylated phospholipid illustrated in Fig. 5.

The biotin-functionalized nanoparticles can be characterized by HABA (4-hydroxyazobenzene-2-carboxylic acid) dye assay [29]. It is known that the combination of HABA and avidin gives a complex that has absorption at 500 nm. When the complex meets with biotin, the strong biotin–avidin interaction will displace HABA from the complex, reducing the absorption at 500 nm. Figure 7A shows the UV–vis spectra of HABA/avidin (0.3 mM HABA, 0.45 mg/mL avidin, 0.3 M NaCl, 0.01 M HEPES (N-[2-hydroxyethyl]piperazine-NH-[2-ethanesulfonic acid], a buffer with pK<sub>a</sub> = 7.5), 0.01 M MgCl<sub>2</sub>, 0.02 % sodium azide (as a preservative)). The 500 nm absorption is clearly seen. When BNPs (~0.25 mg/mL) are added, the intensity of the absorption peak is reduced. From this decrease, we can calculate that the biotin around the BNPs has a concentration equivalent to 70 nmol/mL [27]. This proves that the monodisperse Fe<sub>3</sub>O<sub>4</sub> (or MnFe<sub>2</sub>O<sub>4</sub>) nanoparticles are readily biotinylated. Our further experiments indicate that the particles can be functionalized with a variety of functional groups of not only biotin, but also –COOH, –SH, and –NH<sub>2</sub>, facilitating the attachment of DNAs, proteins, or cells on the surface of the particles.



**Fig. 7** UV-vis spectra of HABA/avidin with stepwise addition of BNPs: (A) HABA/avidin; (B) 18 equiv of A and 1 equiv of BNPs; (C) 18 equiv of A and 2 equiv of BNPs; (D) 18 equiv of A and 3 equiv of BNPs.

## CONCLUSIONS

One-pot reaction of metal acetylacacate with 1,2-alkanediol in the presence of oleic acid and oleylamine leads to the formation of nearly monodisperse magnetic ferrite  $MFe_2O_4$  nanoparticles. The size of the particles is tuned by the reactant concentration and surfactant/metal ratio and  $MFe_2O_4$  nanoparticles with size up to 15 nm have been made via this one-pot reaction process. The process may be considered a more convenient route to ferrite nanoparticles compared to the previous high-temperature solution-phase synthesis and seed-mediated growth method as there is no injection or seeds are required in the reaction. With the fine control of reaction parameters, such as reactant concentration and surfactant/metal ratio, the size, and therefore the magnetic properties, of the particles can be optimized for magnetic sensor detection. Such magnetic nanoparticles, with proper surface functionalization, can be used to attach to target biomolecules and serve as a label for highly sensitive biosensing, separation, and imaging applications.

## ACKNOWLEDGMENTS

The work was supported by DARPA through ONR under Grant Nos. N00014-01-1-0885 and the Salomon Award from Brown University.

## REFERENCES

1. A. H. Morrish. *The Physical Principles of Magnetism*, Chap. 7, John Wiley, New York (1965).
2. K. M. Unruh, C. L. Chien. In *Nanomaterials: Synthesis, Properties and Applications*, A. S. Edelstein, R. C. Cammarata (Eds.), Chap. 14, Institute of Physics Publishing (1996).
3. U. Häfeli, W. Schütt, J. Teller, M. Zborowski. *Scientific and Clinical Applications of Magnetic Carriers*, Plenum Press, New York (1997).
4. Q. A. Pankhurst, J. Connolly, S. K. Jones, J. Dobson. *J. Phys. D: Appl. Phys.* **36**, R167 (2003).
5. P. Tartaj, M. P. Morales, S. Veintemillas-Verdaguer, T. González-Carreño, C. J. Serna. *J. Phys. D: Appl. Phys.* **36**, R182 (2003).
6. P. Tartaj, M. P. Morales, T. González-Carreño, S. Veintemillas-Verdaguer, C. J. Serna. *J. Magn. Mater.* **290-291**, 28 (2005).
7. T. Neuberger, B. Schöpf, H. Hofmann, M. Hofmann, B. von Rechenber. *J. Magn. Mater.* **293**, 483 (2005).

8. O. Bomati-Miguel, M. P. Morales, P. Tartaj, J. Ruiz-Cabello, P. Bonville, M. Santos, X. Zhao, S. Veintemillas-Verdaguer. *Biomaterials* **26**, 5695 (2005).
9. H. T. Song, J. S. Choi, Y. M. Huh, S. Kim, Y. W. Jun, J. S. Suh, J. Cheon. *J. Am. Chem. Soc.* **127**, 9992 (2005).
10. Y. M. Huh, Y. W. Jun, H. T. Song, S. Kim, J. S. Choi, J. H. Lee, S. Yoon, K. S. Kim, J. S. Shin, J. S. Suh, J. Cheon. *J. Am. Chem. Soc.* **127**, 12387 (2005).
11. S. Sun, H. Zeng. *J. Am. Chem. Soc.* **124**, 8204 (2002).
12. S. Sun, H. Zeng, D. B. Robinson, S. Raoux, P. M. Rice, S. X. Wang, G. Li. *J. Am. Chem. Soc.* **126**, 273 (2004).
13. Q. Song, Z. J. Zhang. *J. Am. Chem. Soc.* **126**, 6164 (2004).
14. H. Zeng, P. M. Rice, S. X. Wang, S. Sun. *J. Am. Chem. Soc.* **126**, 11458 (2004).
15. J. Rockenberger, E. C. Scher, A. P. Alivisatos. *J. Am. Chem. Soc.* **121**, 11595 (1999).
16. M. D. Bentzon, J. van Wonterghem, S. Mørup, A. Thölen, C. J. Koch. *Philos. Mag. B* **60**, 169 (1989).
17. Q. Guo, X. Teng, S. Rahman, H. Yang. *J. Am. Chem. Soc.* **125**, 630 (2003).
18. F. X. Redl, K.-S. Cho, C. B. Murray, S. O'Brien. *Nature* **423**, 968 (2003).
19. T. Hyeon, Y. Chung, J. Park, S. S. Lee, Y.-W. Kim, B. H. Park. *J. Phys. Chem. B* **106**, 6831 (2002).
20. J. Park, K. An, Y. Hwang, J.-G. Park, H.-J. Noh, J.-Y. Kim, J.-H. Park, N.-M. Hwang, T. Hyeon. *Nat. Mater.* **3**, 891 (2004).
21. J. Park, E. Lee, N.-M. Hwang, M. Kang, S. C. Kim, Y. Hwang, J.-G. Park, H.-J. Noh, J.-Y. Kim, J.-H. Park, T. Hyeon. *Angew. Chem., Int. Ed.* **44**, 2872 (2005).
22. D. H. Everett. *Basic Principles of Colloid Science*, Chap. 4, Royal Society of Chemistry, London (1988).
23. A. R. West. *Basic Solid State Chemistry*, pp. 356–359, John Wiley, New York (1988).
24. T. Y. Kim, M. S. Lee, Y. I. Kim, C.-S. Lee, J. C. Park, D. Kim. *J. Phys. D: Appl. Phys.* **36**, 1451 (2003).
25. G. Li, V. Joshi, R. L. White, S. X. Wang, J. T. Kemp, C. Webb, R. W. Davis, S. Sun. *J. Appl. Phys.* **93**, 7557 (2003).
26. G. Li, S. Wang, S. Sun. *IEEE Trans. Magn.* **40**, 3000 (2004).
27. X. Michalet, F. F. Pinaud, L. A. Bentolila, J. M. Tsay, S. Doose, J. J. Li, G. Sundaresan, A. M. Wu, S. S. Gambhir, S. Weiss. *Science* **307**, 538 (2005).
28. I. L. Medintz, H. T. Uyeda, E. R. Goldman, H. Mattoussi. *Nat. Mater.* **4**, 435 (2005).
29. N. M. Green. *Methods Enzymol.* **18A**, 418 (1970).